Pyrazine-interior-embodied MOF-74 for selective CO_2 adsorption

meng zhao[1], Yujie Ban[1], Ze Chang[2], Yingwu Zhou[1], Kun Yang[1], Yuecheng Wang[1], Na Cao[1], and Weishen Yang[1]

[1]Dalian Institute of Chemical Physics
[2]Nankai University

May 3, 2021

Abstract

A series of pyrazine-interior-embodied MOF-74 composites (py-MOF-74) were successfully synthesized by a post vapor modification method, concomitant with the loading ratio of pyrazine easily controlled in this process. Here, pyrazine molecules perform as a cavity-occupant to block the wide pores of MOF-74, which accentuates the adsorption discrepancy of a pair of gases on MOFs and consequently reinforces the adsorption selectivity (typically for CO_2/N_2, CO_2/CH_4). Different from the "physical confinement" of occupants, pyrazine molecule with dual "para-nitrogen" atoms donates one N atom to bond with the open metal ion of MOF-74 for stability, and remains the other N atom available for potential CO_2 trapping site. Pyrazine-interior-embodied MOF-74 composites manifest significantly improved CO_2/N_2 and CO_2/CH_4 adsorption selectivity. Typically, py-MOF-74c with ultimate pyrazine insertion displays selectivity greatly superior to MOF-74 in the equimolar CO_2/CH_4 (598 vs. 35) and the simulated CO_2/N_2 flue gas (471 vs. 49) at 100 kPa and 298 K.

Pyrazine-interior-embodied MOF-74 for selective CO_2 adsorption

Meng Zhao[1,2] | Yujie Ban[1,5]* (0000-0002-7336-8514) | Ze Chang[3,4] | Yingwu Zhou[1,2]| Kun Yang[1,2] | Yuecheng Wang[1,2] | Na Cao[1,2]| Weishen Yang[1,2]* (0000-0001-9615-7421)

[1] State Key Laboratory of Catalysis, Dalian Institute of Chemical Physics, Chinese Academy of Sciences, Dalian 116023, China.

[2] University of Chinese Academy of Sciences, Beijing 100049, China.

[3] School of Materials Science and Engineering, National Institute for Advanced Materials, TKL of Metal and Molecule-Based Material Chemistry, Nankai University, Tianjin, 300350 P. R. China

[4] Collaborative Innovation Center of Chemical Science and Engineering (Tianjin), Tianjin, 300072 P. R. China

[5] Dalian National Laboratory for Clean Energy, Dalian 116023, China.

*Corresponding authors:

E-mail: yjban@dicp.ac.cn (Yujie Ban)

E-mail: yangws@dicp.ac.cn (Weishen Yang)

Abstract

A series of pyrazine-interior-embodied MOF-74 composites (py-MOF-74) were successfully synthesized by a post vapor modification method, concomitant with the loading ratio of pyrazine easily controlled in this process. Here, pyrazine molecules perform as a cavity-occupant to block the wide pores of MOF-74, which accentuates the adsorption discrepancy of a pair of gases on MOFs and consequently reinforces the adsorption

selectivity (typically for CO_2/N_2, CO_2/CH_4). Different from the "physical confinement" of occupants, pyrazine molecule with dual "para-nitrogen" atoms donates one N atom to bond with the open metal ion of MOF-74 for stability, and remains the other N atom available for potential CO_2 trapping site. Pyrazine-interior-embodied MOF-74 composites manifest significantly improved CO_2/N_2 and CO_2/CH_4 adsorption selectivity. Typically, py-MOF-74c with ultimate pyrazine insertion displays selectivity greatly superior to MOF-74 in the equimolar CO_2/CH_4 (598 vs. 35) and the simulated CO_2/N_2 flue gas (471 vs. 49) at 100 kPa and 298 K.

Keywords: Metal-organic frameworks, pyrazine-interior-embodied composites, cavity-occupying, selective adsorption, CO_2capture

1 | Introduction

Carbon dioxide capture is an effective strategy to mitigate greenhouse effect and other related challenges. CO_2/N_2 separation technology is pivotal for post-combustion CO_2 capture since the flue gas from power plants is mainly composed of N_2(70%~75%) and CO_2(10%~15%) [1]. Besides, CO_2 is also a harmful component for natural gas, especially under moisture condition [2]. Therefore, separation of CO_2 from CH_4 is challenging but of great significance to methane upgrading[3]. Compared with traditional amine-scrubbing, adsorptive separation employing suitable porous materials is sought-after as a result of the ease of operation and low energy expenditure.

Metal-organic frameworks (MOFs) are promising adsorbents for their diversified chemical compositions and porous skeletons[4-6]. The advancement of MOFs has motivated their utility in gas separation and purification [7-13]. Selective adsorption on MOFs underpins isolating gases in high purity. The core is to significantly accentuate the adsorption discrepancy of a pair of gases (e.g., CO_2/N_2, CO_2/CH_4) on MOFs, which is critical for selectivity in dynamic adsorption-based separation and membrane separation [14-18]. Cavity-occupying is an efficient solution to narrow the pore size, and thereby to reinforce the molecular recognition and selective adsorption of MOFs while retaining structural integrity. This operation would be more effective in MOFs with flexibility or with pore size significantly larger than molecule dimensions. Ban et al. demonstrated that the confinement of ionic liquid [bmim][Tf_2N] into the sodalite nanocage of ZIF-8 can tailor the cage size of ZIF-8, impeding the passage of the larger molecule and appreciably improve CO_2/N_2selectivity from 19 to 100 [19]. Liao et al. decorated hydrazine into the pore of a MOF. The composite also excels in selective adsorption of CO_2 at low pressure [20]. Lin et al. loaded molecular-level polyethyleneimine into the nanopore of MIL-101, engendering lower CO_2 capacity but higher CO_2/N_2 selectivity in the constrained inner pore space [21].

MOF-74 possessing abundant open metal sites take up significant saturable CO_2 capacity. However, the large pore of MOF-74 displays moderate CO_2 selectivity over N_2 and CH_4 [22]. It is worthy to explore the possibility of improving CO_2selectivity by cavity-occupying. Nitrogen-containing agents show good CO_2 affinity in terms of Lewis acid-base interactions but weaker binding with CH_4 and N_2 [23]. Therefore, introduction of the suitable nitrogen-containing agent as a cavity-occupant could be helpful for reducing the effective pore size of MOF-74, and simultaneously providing compensation sites for CO_2 trapping. In this work, we seek to demonstrate a platform based on MOF-74 for outstanding CO_2 selective adsorption. Pyrazine with dual "para-nitrogen" atoms was introduced into the pore of MOF-74 via a post vapor modification method (Scheme 1). One nitrogen atom of pyrazine is bonded to the open metal ions in MOF-74 with a minimal steric hindrance, and the other nitrogen atom of pyrazine provides potential affinity to CO_2, resulting in a stable pyrazine-interior-embodied MOF-74 composite for boosting CO_2/N_2 and CO_2/CH_4 adsorption selectivity through varying the pyrazine loading content. Given the pore environment of MOF-74 after pyrazine modification, the selective adsorption of pyrazine-interior-embodied MOF-74 for C_4olefine/paraffine was also investigated.

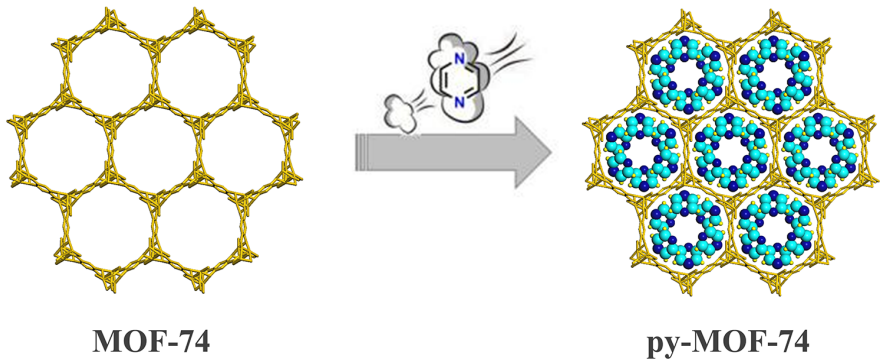

Scheme 1 A post vapor modification process to produce pyrazine-interior-embodied MOF-74.

2 | Experiment section

2.1 | Materials

Chemical reagents were commercially available and used without further purification. $Co(NO_3)_2{\cdot}6H_2O$ (98%) was obtained from Sigma-Aldrich. Pyrazine (99%) and 2,5-dihydroxyterephthalic acid (97%) were provided by Shanghai Aladdin Bio-Chem Technology Co., LTD. N, N-dimethylformamide (DMF, AR), ethanol (AR) and methanol (AR) were obtained from Sinopharm Group Co., LTD.

2.2 | Preparation of MOF-74 and py-MOF-74

Synthesis of MOF-74. Co-MOF-74 crystals were achieved by reaction of $Co(NO_3)_2{\cdot}6H_2O$ (1.03 mmol) and 2,5-dihydroxyterephthalic acid (dhtp, 0.330 mmol) in a mixed solvent (DMF/ethanol/water = 1: 1: 1 in volume, 24 mL in total) under a solvothermal condition (at 100°C for 24 h). Fresh-synthesized Co-MOF-74 were activated at 250 under a vacuum system for 12 h to generate open metal sites.

Synthesis of py-MOF-74. The activated MOF-74 was immediately transferred into a stainless-steel autoclave containing a certain amount of pyrazine in the glovebox filled with N_2. The autoclave was heated at 110 for 1 d, in which MOF-74 was soaked in the high-density of pyrazine steam, producing pyrazine-interior-embodied MOF-74 (py-MOF-74). The pyrazine amount in the autoclave was changed in the post vapor modification process, resulting in the reactive molar ratio of Co^{2+} nodes in MOF-74 to pyrazine of 1: 0.5 for py-MOF-74a, 1: 1 for py-MOF-74b and 1: 10 for py-MOF-74c. After 24 h, py-MOF-74 was washed with methanol to remove the weakly binding pyrazine molecules, and treated under vacuum condition for sample activation.

2.3 | Structural characterizations

The X-ray diffraction (XRD) patterns were performed on Rigaku D/MAX 2500/PC with Cu Kα radiation (λ=0.154 nm at 40 kV and 200 mA). The patterns were collected from 2° to 50° with a 5° min^{-1}scan speed at a normal pressure and room temperature. For thermogravimetric (TG) measurements, samples were treated with a heating rate of 10°C min^{-1} from 40°C to 750°C on a Netzsch STA 449F3 instrument under a 20 mL min^{-1} of N_2 flow. Fourier Transform Infrared (FTIR) spectra from 400 to 4000 cm^{-1} were recorded on a Thermofisher Scientific Nicolet iS50 spectrometer.

2.4 | Gas adsorption experiments

Gas adsorption at 0-110 kPa was conducted on a Micromeritics ASAP 2020 Plus physisorption analyzer. The adsorption isotherms of gases were fitted with the dual-site Langmuir-Freundlich model (eq. 1)

$$q=\frac{q_1k_1p^{v_1}}{1+k_1p^{v_1}}+\frac{q_2k_2p^{v_2}}{1+k_2p^{v_2}} \quad \text{(eq. 1)}$$

Where q (mmol g^{-1}) is the saturation adsorption amount,q_1 and q_2 (mmol g^{-1}) is the saturation capacity

on site 1 and site 2 of the adsorbent, respectively. The constant k_1(kPa^{-1}) and k_2(kPa^{-1}) represents the affinity coefficient for site 1 and 2, and v_1 and v_2 stands for the deviations of site 1 and site 2 from an ideally homogeneous surface, respectively. The variable p(kPa) is the total gas pressure. Based on ideal adsorbed solution theory (IAST), adsorption selectivity of gas was predicted according to the following equation (eq. 2) [24,25].

$$S_{a/b}=\frac{x_a/y_a}{x_b/y_b} \quad \text{(eq. 2)}$$

Where x_a and x_b are the molar fraction of component a and b in the adsorbed state, respectively, and y_a and y_b are the molar fraction of component a and b in the gas state, respectively.

Virial equation (eq. 3) was employed to demonstrate the enthalpies of adsorption based on isotherms at two different temperature (298 K and 273 K) [25].

$$\ln p = \ln N + 1/T \sum_{i=0}^{m} a_i N^i + \sum_{j=0}^{n} b_j N^j \quad \text{(eq. 3)}$$

Here, p is the pressure expressed in Pa, N is the amount absorbed in mol g^{-1}, T is the temperature in K, a_i and b_j are Virial coefficients, and m , n represent the number of coefficients required to adequately describe the isotherms. The values of the Virial coefficients a_0 through a_m were then used to calculate enthalpies (Q_{st}) of absorption using (eq. 4)[25].

$$Q_{st} = -R \sum_{i=0}^{m} a_i N^i \quad \text{(eq. 4)}$$

3 | Results and discussion

3.1 | Characterizations of py-MOF-74

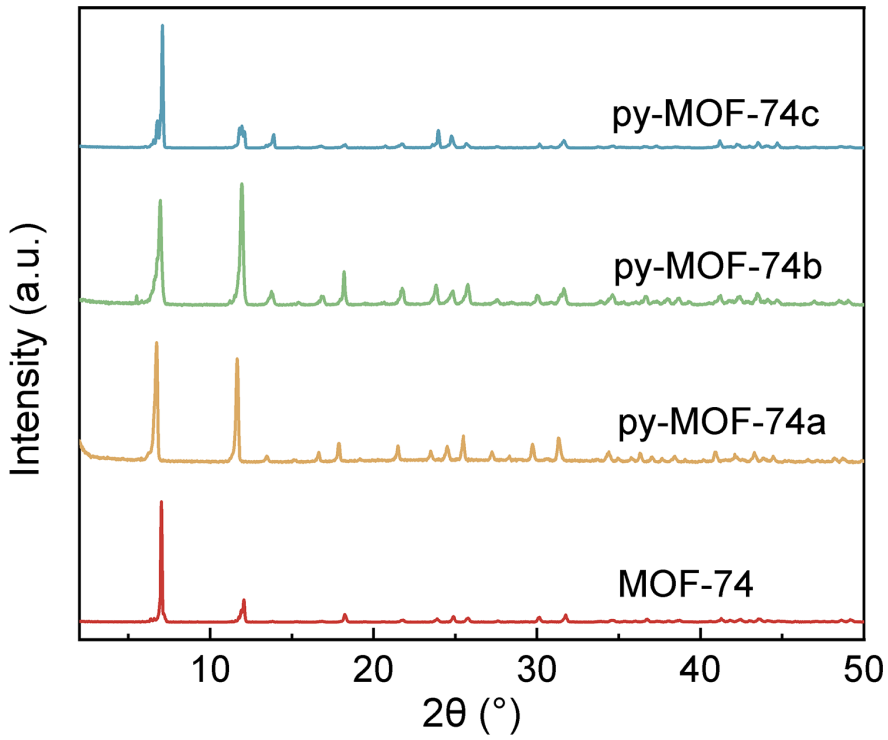

Figure 1 PXRD patterns of MOF-74 and py-MOF-74.

PXRD of MOF-74 show typical dominated diffraction peaks at 2ϑ of 7° and 12°, which is consistent with the simulated pattern obtained from the single-crystal structure. Pyrazine-modified MOF-74, namely py-MOF-74a, py-MOF-74b and py-MOF-74c show featured diffraction peaks analogous with that of MOF-74, indicative of no loss of crystallinity after pyrazine modification (Figure 1).

The pristine MOF-74 crystal maintains stability with a tiny weight loss before ˜420°C. An incipient structural decomposition appears at the higher temperature. Modified MOF-74 crystals show negligible weight loss below 250°C (Figure 2a), which has been beyond the vaporization temperature of pyrazine (115°C at 1 atm). It suggests that pyrazine molecules are embodied into the framework of MOF-74 by chemical bonds. It is worth mentioning that the introduction of pyrazine molecules improves the thermal stability of the MOF-74 framework; a significant weight loss appears after 500°C. In the light of above analysis, the weight loss of py-MOF-74 before this temperature, corresponding to the pyrazine removal, was utilized to estimate the pyrazine loading ratio. The weight loss for py-MOF-74a, py-MOF-74b and py-MOF-74c is 16.4, 26.0% and 33.9%, respectively, which can be translated into py-MOF-74 with the formula of $Co_2(dhtp)(py)_{0.765}$, $Co_2(dhtp)(py)_{1.37}$ and $Co_2(dhtp)(py)_{2.00}$. Py-MOF-74c permits one pyrazine molecule insert to one open metal site, giving the highest pyrazine loading content. A vibration peak at 440 cm^{-1}in FTIR spectra of pyrazine modified MOF-74 can be assignable to the formation of Co-N bonds (Figure 2b). And the peak becomes strong with the increase of pyrazine content. It further indicates that pyrazine molecules are bonded to the open metal sites [Co (II)] of MOF-74, forming pyrazine-interior-embodied composites. N_2 adsorption isotherms were measured at 77K (Figure 3a). The parent framework and modified MOF-74, except for py-MOF-74c, exhibit typical Type-I adsorption isotherms: a steep adsorption behavior at the relative pressure $P/P_0 < 0.01$ with the saturation capacity reaching 316, 138 and 68 cm^3g^{-1} for MOF-74, py-MOF-74a and py-MOF-74b, respectively. Owing to the blocking effect, N_2 can hardly access to the py-MOF-74c with the highest pyrazine loading. Accordingly, the Brunauer-Emmett-Teller (BET) surface area is 605, 300 and 42 m^2 $g^{-1}$for py-MOF-74a, py-MOF-74b and py-MOF-74c, which is inferior to parent MOF-74 (1358 m^2 g^{-1}). The block effect arising from pyrazine molecules also leads to a significant shift of pore size distribution

(PSD) from 9.85 nm (MOF-74) to 9.28 nm (py-MOF-74a). Further increasing the loading of pyrazine, the pore volume of py-MOF-74b and py-MOF-74c sharply shrinks, along with the PSD almost undetectable by the current gas probe. We suppose the existence of extremely narrow pores in py-MOF-74, which are inaccessible to N_2 molecule.

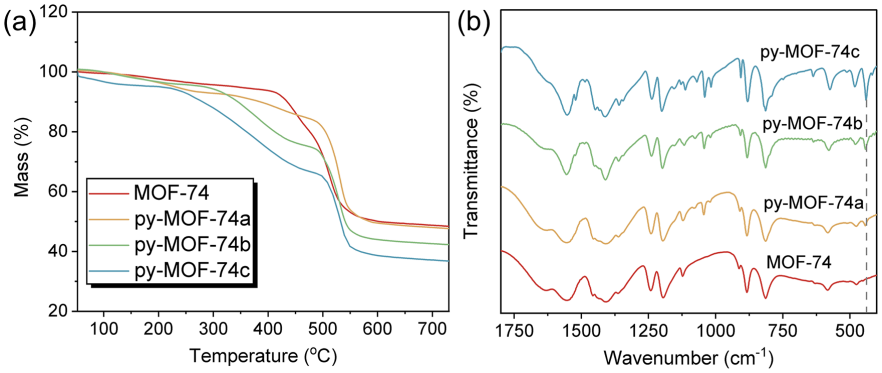

Figure 2 TG curves (a) and FTIR spectra (b) of MOF-74 and py-MOF-74.

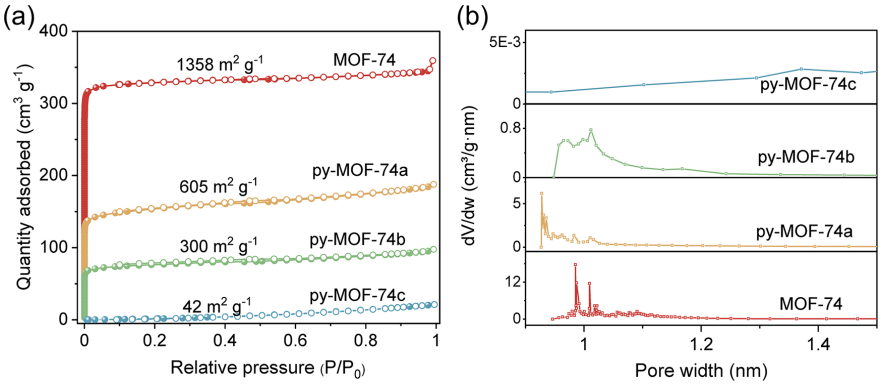

Figure 3 Nitrogen adsorption isotherms of MOF-74 and py-MOF-74 at 77 K (a) and corresponding PSDs analyzed by Horvath-Kawazoe method (b).

3.2 | Selective adsorption of CO_2 onpy-MOF-74

3.2.1 | Adsorption isotherms

Gas adsorption of CO_2, CH_4 and N_2 executed on MOF-74 and py-MOF-74 at 298 K are depicted in Figure 4. The isotherms were fitted by the dual-site Langmuir-Freundlich model (Table S1-S4). As shown in Figure 4a, the uptake capacity of CO_2 amounts to 6.65 mmol g^{-1} (29.3 wt.%) at 100 kPa, whereas it adsorbs relatively low quantity of CH_4 (1.25 mmol g^{-1}, 5.50 wt %) and N_2 (0.65 mmol g^{-1}, 2.86 wt.%). The adsorption properties of pyrazine-interior-embodied MOF-74 were further examined. As shown in Figure 4b-4d, the uptake capacity of CO_2 at 298 K is 2.32 mmol g^{-1}(10.21 wt.%) and 1.35 mmol g^{-1} (5.95 wt.%) for py-MOF-74a and py-MOF-74b, respectively, presenting a proportional correlation with the BET surface area of materials (as shown in Figure 5). Nevertheless, the saturation uptake of py-MOF-74c at 100 kPa reaches 1.07 mmol g^{-1} (4.71 wt.%), far beyond the theoretically anticipated value, which indicates that the inserted pyrazine with one dangling N atom can be available as a compensation site for trapping CO_2 by terms of Lewis acid-base interactions. This value is also comparable to the saturation uptake of some well-known MOF materials at 100 kPa and 298 K, such as ZIF-8 (3.30 wt.%)[19], ZIF-95 (3.87 wt.%) and ZIF-100 (4.21

wt.%)[26]. Besides, py-MOF-74c exhibits a steep adsorption behavior below 10 kPa over py-MOF-74a and py-MOF-74b, which further proves the special affinity of this composite to CO_2. Owing to the pyrazine blocking effect, the adsorption capacity of larger molecules CH_4 and N_2 on modified MOF-74 also significantly reduces.

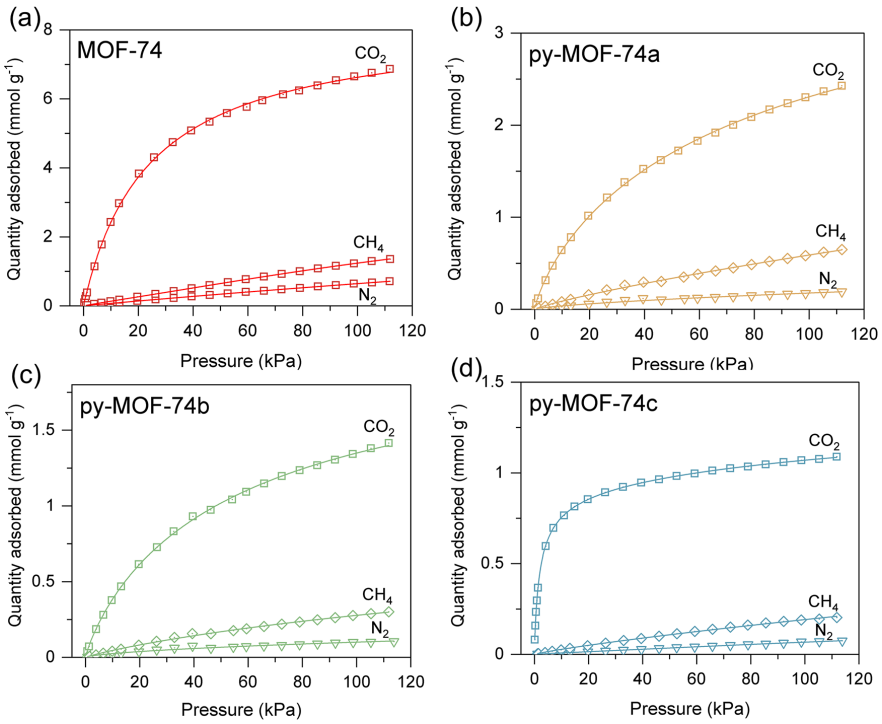

F igure 4CO_2, CH_4 and N_2adsorption isotherms of MOF-74 and py-MOF-74 at 298 K. Symbols and solid lines denote experimental points and curves fitted by dual-site Langmuir-Freundlich model, respectively.

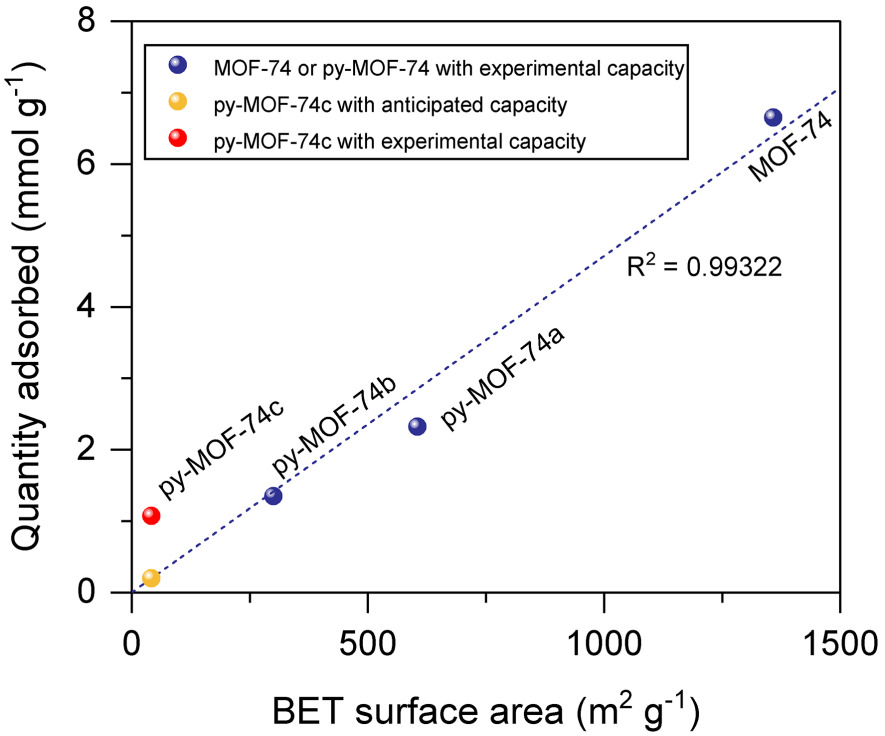

Figure 5 The proportional correlation between CO_2 uptake capacity with the BET surface area of materials. The dash line is fitted by using the experimental results of MOF-74, py-MOF-74a and py-MOF-74c.

3.2.2 | Zero coverage adsorptionenthalpies

Adsorption enthalpies (Q_{st}) were determined by Virial equation (Figure S1-S6) based on single-component isotherms at 298 K and 273 K. The zero coverage Q_{st} of CO_2 on MOF-74 and py-MOF-74 is higher than that of CH_4 and N_2, indicating special affinity of $CO_2$to frameworks. The zero coverage Q_{st} of CO_2 on MOF-74 is 33.6 kJ mol^{-1}. The zero coverage Q_{st} shows a drop trend with the introduction of py (Table 1), since the open metal sites were partially or completely capped by pyrazine molecules. Furthermore, the lowest zero coverage Q_{st} of CO_2 appears on py-MOF-74c with ultimate pyrazine insertion. It provides an indirect proof of pyrazine positioning into the parent framework. In short, the zero coverageQ_{st} of py-MOF-74 for CO_2 is moderate, which would facilitate the effective diffusion and regeneration processes. This trait is important for practical adsorption and membrane separation.

Table 1 Zero coverage adsorption enthalpies (Q_{st}) of CO_2, N_2 and CH_4 on MOF-74 and py-MOF-74

Hosted file

`image7.emf` available at https://authorea.com/users/411483/articles/520494-pyrazine-interior-embodied-mof-74-for-selective-co2-adsorption

3.2.3 | CO_2/CH_4 and CO_2/N_2 adsorption selectivity

Adsorption selectivity of $CO_2/CH_4$and CO_2/N_2 predicted on the basis of IAST was employed to evaluate the competitive adsorption potential of pyrazine-interior-embodied MOF-74. As shown in Figure 6a, the adsorption selectivity of py-MOF-74a and py-MOF-74b for the equimolar binary CO_2/CH_4 is 9.8 and 19.9 at 100 kPa, respectively, lower than the parent MOF-74. However, further increasing the pyrazine content is profitable to the improvement of selectivity of CO_2/CH_4. Py-MOF-74c with ultimate pyrazine insertion displays the highest selectivity (598), which is 17 times of that of parent MOF-74. It suggests that the molecular sieve effect dominates the CO_2 selectivity in this case. Furthermore, py-MOF-74c shows overwhelming

advantages over other MOFs in adsorptive CO_2/CH_4 selectivity, for instance, ZU-66 with selectivity of 136 [27], Co-btz-ht with selectivity of 63 [28] and IRH-3 with selectivity of 27[29] at 298 K. Pyrazine-bonded into the MOF-74 framework can also significantly widen the adsorption gaps between CO_2 and N_2 as a result of their differences in boiling point and polarizability besides molecular size (Table 2). The three modified materials show significantly higher adsorption selectivity than the original material for CO_2/N_2 (Figure 6b and 6c). For 50: 50 CO_2/N_2 mixture, pyrazine modified materials show the adsorption selectivity greatly superior to MOF-74, for example, py-MOF-74c with selectivity of 451 at low pressure (40 kPa) (Figure 6b and 6c). Unexpectedly, for py-MOF-74b with the moderate pyrazine loading, the competitive adsorption effect between CO_2 and N_2 can be amplified with the increase of pressure. The adsorption selectivity of CO_2/N_2 for py-MOF-74b reaches 1711 at 100 kPa and 298 K, which is 35 times of that of MOF-74 and much higher than that of the famous MOFs used for CO_2 selective adsorption, such as an exceptional candidate PCN-200 (260, at 296 K) [30]. Moreover, for 15: 85 CO_2/N_2 (simulated flue-gas) mixture, py-MOF-74c also exhibits the optimal adsorption selectivity. For example, the adsorption selectivity at 100 kPa and 298 K follows the order of py-MOF-74c (471) > py-MOF-74b (147) > py-MOF-74a (87) > MOF-74 (49). In brief, the competitive adsorption potential of py-MOF-74c for CO_2 over N_2 is greatly superior to previously reported MOFs at analogous conditions, such as NJFU-2a (195) [31], Zn(imPim) (106) [32] and BTU-11 (43)[33]. These results indicate that pyrazine-interior-embodied MOF-74 display exceptionally selective CO_2 adsorption properties, which make them good candidates for MOF membrane materials and nanofillers of mixed matrix membranes that are implemented in dynamic CO_2separations.

Table 2 Physical parameters [34] of CO_2, N_2 and CH_4

Hosted file

`image8.emf` available at https://authorea.com/users/411483/articles/520494-pyrazine-interior-embodied-mof-74-for-selective-co2-adsorption

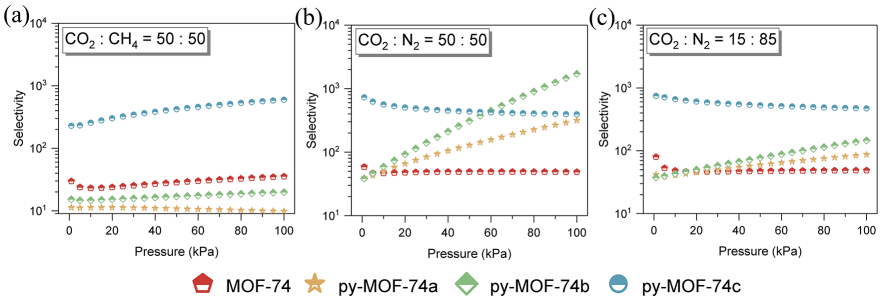

Figure 6 Adsorption selectivity of MOF-74 and py-MOF-74 predicted by IAST for the binary mixture with the specific molar ratio at 298 K.

3.3 | Selective adsorption of C_4 olefine on py-MOF-74

Considering the basic nature of dangling N atom of pyrazine, we envisage that py-MOF-74 with narrow pores could enable selective adsorption of more acidic but smaller olefine instead of paraffine. Accordingly, pure-component isotherms were collected at 298 K to investigate the selective adsorption properties of C_4 olefine on py-MOF-74 and their separation potential of C_4 olefine from paraffine, processes that are relevant for petrochemical industries. Figure 7a reveals Type-I isotherms of olefine and paraffine on MOF-74 and py-MOF-74. MOF-74 displays a tiny adsorption difference between n-butene and n-butane. As a result of the block effect of pyrazine, the absolute capacity of gas molecules reduces, which is similar with the CO_2adsorption result. However, the adsorption difference of py-MOF-74a for n-butene and n-butane becomes obvious. According to the IAST prediction (Figure 7b, Table S5-S7), the optimal ideal adsorption selectivity of n-butene over n-butane appears at py-MOF-74a (Figure 7b), which is distinct from the CO_2 selective adsorption results. For the selective adsorption of the larger C_4 olefine, on the one hand, py-MOF-

74a with the lowest pyrazine loading content and thereby suitable pore space displays affinity to more acidic n-butene over n-butane. On the other hand, the narrowing pore space of py-MOF-74a, compared with the parent framework, could distinguish the molecular difference of n-butene and n-butane (kinetic diameter, 0.446 nm versus 0.469 nm)[35], widening the adsorption gaps between these two molecules. Therefore, the adsorption selectivity of n-butene/n-butane increases from 0.7 (MOF-74) to 3.4 (py-MOF-74a).

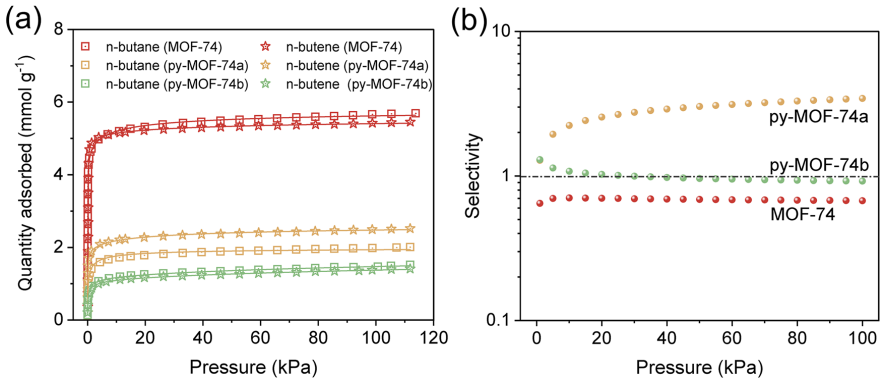

Figure 7 Adsorption isotherms of n-butane and n-butene on MOF-74 and py-MOF-74 at 298 K (a) and the corresponding n-butene/n-butane adsorption selectivity for the equimolar binary mixture at 298 K predicted by IAST (b).

4 | Conclusions

In summary, pyrazine-interior-embodied MOF-74 composites were prepared through a post vapor modification process. Owing to the blocking effect of pyrazine molecules, the composites can significantly widen the adsorption gaps between CO_2 and its counterparts (CH_4 and N_2), resulting in lower saturation uptake for gases albeit with much higher selectivity. We also underline the stability of pyrazine-interior-embodied MOF-74. Pyrazine molecules can hardly escape from the composites at its boiling point, and the composites display higher thermal stability than the parent framework MOF-74, which is attributed to the chemical insertion of pyrazine to the open metal ions of MOF-74. The pyrazine-interior-embodied MOF-74 composites that display significant CO_2 selectivity and moderate adsorption enthalpies would be good candidates in dynamic adsorption-based separation and membrane separation.

Acknowledgements

We thank XianHe Bu's group from Nankai University for the assistance in calculation of adsorption selectivity and enthalpies. This work was supported by the National Natural Science Foundation of China (21706249, 22090060/22090063 and 21978283), Strategic Priority Research Program of Chinese Academy of Sciences (grant XDB17020400), LiaoNing Revitalization Talents Program (XLYC1801004), Youth Innovation Promotion Association CAS and the DNL Cooperation Fund, CAS (DNL201920).

Conflict of interest

The authors declare no potential conflict of interest.

References

1. Gao W, Liang S, Wang R, et al. Industrial carbon dioxide capture and utilization: state of the art and future challenges. *Chem Soc Rev.* 2020;49:8584-8686.

2. Chung WC, Chang MB. Review of catalysis and plasma performance on dry reforming of CH_4 and possible synergistic effects. *Renew Sust Energ Rev.* 2016;62:13-31.

3. Cui W-G, Hu T-L, Bu X-H. Metal–organic framework materials for the separation and purification of light hydrocarbons. *Adv Mater.* 2020;32:1806445.

4. Hosono N, Kitagawa S. Modular design of porous soft materials via self-organization of metal–organic cages. *Acc Chem Res.* 2018;51:2437-2446.

5. Kitagawa S, Matsuda R. Chemistry of coordination space of porous coordination polymers. *Coord Chem Rev.* 2007;251:2490-2509.

6. Chen B, Eddaoudi M, Hyde ST, Keeffe M, Yaghi OM. Interwoven metal-organic framework on a periodic minimal surface with extra-large pores. *Science.* 2001;291:1021.

7. Liao P-Q, Huang N-Y, Zhang W-X, Zhang J-P, Chen X-M. Controlling guest conformation for efficient purification of butadiene.*Science.* 2017;356:1193.

8. Li L, Lin R-B, Krishna R, et al. Ethane/ethylene separation in a metal-organic framework with

iron-peroxo sites. *Science* 2018;362:1443-446.

9. Hou Q, Zhou S, Wei Y, Caro J, Wang H. Balancing the grain boundary structure and the framework flexibility through bimetallic metal–organic framework (MOF) membranes for gas separation. *J Am Chem Soc.* 2020;142:9582-9586.

10. Lyndon R, You W, Ma Y, et al. Tuning the structures of metal–organic frameworks via a mixed-linker strategy for ethylene/ethane kinetic separation. *Chem Mater.*2020;32:3715-3722.

11. Rodenas T, Luz I, Prieto G, et al. Metal–organic framework nanosheets in polymer composite materials for gas separation. *Nat Mater.* 2015;14:48-55.

12. Bae T-H, Lee JS, Qiu W, Koros WJ, Jones CW, Nair S. A high-performance gas-separation membrane containing submicrometer-sized metal–organic framework crystals. *Angew Chem Int Ed.*2010;49:9863-9866.

13. Li Y-S, Liang F-Y, Bux H, Feldhoff A, Yang W-S, Caro J. Molecular sieve membrane: Supported metal–organic framework with high hydrogen selectivity. *Angew Chem Int Ed.* 2010;49:548-551.

14. Hu Y, Wei J, Liang Y, et al. Zeolitic imidazolate framework/graphene oxide hybrid nanosheets as seeds for the growth of ultrathin molecular sieving membranes. *Angew Chem Int Ed.*2016;55:2048-2052.

15. Liu Q, Wang N, Caro J, Huang A. Bio-inspired polydopamine: A versatile and powerful platform for covalent synthesis of molecular sieve membranes. *J Am Chem Soc.* 2013;135:17679-17682.

16. Liu G, Chernikova V, Liu Y, et al. Mixed matrix formulations with MOF molecular sieving for key energy-intensive separations. *Nat Mater.* 2018;17:283-289.

17. Song Q, Nataraj SK, Roussenova MV, et al. Zeolitic imidazolate framework (ZIF-8) based polymer nanocomposite membranes for gas separation. *Energy Environ Sci.* 2012;5:8359-8369.

18. Wang Y, Jin H, Ma Q, et al. A MOF glass membrane for gas separation. *Angew Chem Int Ed.* 2020;59:4365-4369.

19. Ban Y, Li Z, Li Y, et al. Confinement of ionic liquids in nanocages: Tailoring the molecular sieving properties of ZIF-8 for membrane-based CO_2 capture. *Angew Chem Int Ed.*2015;54:15483-15487.

20. Liao P-Q, Chen X-W, Liu S-Y, et al. Putting an ultrahigh concentration of amine groups into a metal–organic framework for CO_2 capture at low pressures. *Chem Sci.*2016;7:6528-6533.

21. Lin Y, Lin H, Wang H, et al. Enhanced selective CO_2 adsorption on polyamine/MIL-101(Cr) composites.*J Mater Chem A.* 2014;2:14658-14665.

22. Suh BL, Lee S, Kim J. Size-matching ligand insertion in MOF-74 for enhanced CO_2 capture under humid conditions.*J Phys Chem C.* 2017;121:24444-24451.

23. Kang M, Kang DW, Hong CS. Post-synthetic diamine-functionalization of MOF-74 type frameworks for effective carbon dioxide separation. *Dalton Trans.* 2019;48:2263-2270.

24. Chen Y-Q, Qu Y-K, Li G-R, et al. Zn(II)-benzotriazolate clusters based amide functionalized porous coordination polymers with high CO_2 adsorption selectivity. *Inorg Chem.*2014;53:8842-8844.

25. Li N, Chang Z, Huang H, et al. Specific K^+ binding sites as CO_2 traps in a porous MOF for enhanced CO_2 selective sorption.*Small.* 2019;15:1900426.

26. Wang B, Côté AP, Furukawa H, O'Keeffe M, Yaghi OM. Colossal cages in zeolitic imidazolate frameworks as selective carbon dioxide reservoirs. *Nature.* 2008;453:207-211.

27. Yang L, Cui X, Zhang Y, et al. Anion pillared metal–organic framework embedded with molecular rotors for size-selective capture of CO_2 from $CH_4$and N_2. *ACS Sustain Chem Eng.* 2019;7:3138-3144.

28. Li S, Zeng S, Tian Y, Jing X, Sun F, Zhu G. Two flexible cationic metal-organic frameworks with remarkable stability for CO_2/CH_4 separation. *Nano Res.*2021;https://doi.org/10.1007/s12274-021-3329-8.

29. Mohan M, Essalhi M, Durette D, et al. A rational design of microporous nitrogen-rich lanthanide metal–organic frameworks for CO_2/CH_4 separation. *ACS Appl Mater Interfaces.* 2020;12:50619-50627.

30. Wriedt M, Sculley JP, Yakovenko AA, et al. Low-energy selective capture of carbon dioxide by a pre-designed elastic single-molecule trap. *Angew Chem Int Ed.* 2012;51:9804-9808.

31. Du L, Lu Z, Ma M, Su F, Xu L. A porous cobalt-based MOF with high CO_2 selectivity and uptake capacity. *Rsc Adv.* 2015;5:29505-29508.

32. Wang Z-S, Li M, Peng Y-L, Zhang Z, Chen W, Huang X-C. An ultrastable metal azolate framework with binding pockets for optimal carbon dioxide capture. *Angew Chem Int Ed.* 2019;58:16071-16076.

33. Wang B, Huang H, Lv X-L, Xie Y, Li M, Li J-R. Tuning CO_2 selective adsorption over N_2 and CH_4 in UiO-67 analogues through ligand functionalization. *Inorg Chem.* 2014;53:9254-9259.

34. Li J-R, Kuppler RJ, Zhou H-C. Selective gas adsorption and separation in metal–organic frameworks. *Chem Soc Rev.*2009;38:1477-1504.

35. Barnett BR, Parker ST, Paley MV, et al. Thermodynamic separation of 1-butene from 2-butene in metal–organic frameworks with open metal sites. *J Am Chem Soc.* 2019;141:18325-18333.

Supporting information

Additional supporting information may be found online in the Supporting Information section at the end of this article.